IGTC-0014

STEADY AND UNSTEADY FLOW EFFECTS OF CIRCUMFERENTIAL GROOVES CASING TREATMENT IN A TRANSONIC COMPRESSOR ROTOR

Chunill HAH

NASA Glenn Research Center,
MS 5-11, Cleveland, Ohio 44135

ABSTRACT

The current paper reports on an investigation of steady and unsteady flow effects of circumferential grooves casing treatment in a transonic compressor rotor. Circumferential grooves casing treatment is used mainly to increase stall margin in axial compressors with a relatively small decrease in aerodynamic efficiency. It is widely believed that flow mechanisms of circumferential grooves casing treatment near stall conditions are not yet well understood even though this treatment has been used widely in real engines. Numerical analysis based on steady Reynolds-averaged Navier-Stokes (RANS) has been the primary tool used to understand flow mechanism for circumferential grooves casing treatment. Although steady RANS explains some flow effects of circumferential grooves casing treatment, it does not calculate all the measured changes in the compressor characteristics. Therefore, design optimization of circumferential grooves with steady RANS has not been very successful. As a compressor operates toward the stall condition, the flow field becomes transient. Major sources of self-generated flow unsteadiness are shock oscillation and interaction between the passage shock and the tip leakage vortex. In the present paper, an unsteady Reynolds-averaged Navier-Stokes (URANS) approach is applied to study the effects of circumferential grooves in a transonic compressor. The results from URANS are compared with the results from RANS and measured data. The current investigation shows that there are significant unsteady flow effects on the performance of the circumferential grooves casing treatment. For the currently investigated rotor, the unsteady effects are of the same magnitude as the steady effects in terms of extending the compressor stall margin.

INTRODUCTION

Circumferential grooves casing treatment is applied to extend compressor operating range with small penalties in aerodynamic efficiency. It has been applied to both subsonic and transonic compressors. An increase in stall margin has been reported for most compressors, although for certain compressors no benefits have been reported. The primary purpose of circumferential grooves is to alter the flow structure near the compressor casing as the compressor operates toward stall limit. Precise steady and/or unsteady flow physics at stall onset are not well understood even for compressors with no casing treatment. Therefore, the underlying flow physics of circumferential grooves near stall operation are not clearly understood either. Currently, the design criteria of circumferential grooves are mainly based on loosely connected experimental data and their applications to different designs are not always valid.

Many studies have been made to investigate the effects of casing treatments on compressor performance (Moore et al. [1971], Prince et al. [1974], Paulon and Dehoudt [1982], Smith and Cumpsty [1985], Fujita and Takata [1985], Lee and Greitzer [1990], Crook et al. [1993], Hall et al. [1996], Rabe and Hah [2002], Chen et al. [2010], and Mueller et al. [2011]). Paulon and Dehoudt [1982] conducted a theoretical investigation of the effects of circumferential grooves casing treatment. Rabe and Hah [2002] investigated circumferential grooves casing treatment applied to the first stage rotor in a modern highly loaded two-stage transonic axial compressor. They found that the local flow incidence near the pressure side of the leading edge is reduced due to the circumferential grooves. Mueller et al. [2007] investigated various circumferential grooves applied to the rotor in a single stage transonic compressor. Particle Imaging Velocimetry (PIV) was applied to measure the detailed steady flow field near and inside circumferential grooves in an axial transonic compressor stage by Mueller et al. [2011].

Although significant progress has been made in non-intrusive measurement techniques, direct measurements of unsteady velocity components in the tip clearance region are still beyond current capabilities. Therefore, numerical approaches have been used to investigate flow mechanisms in the tip clearance region in high speed compressors. Most previous numerical studies are based on the steady Renolds-averaged Navier-Stokes (RANS) approach. It has been observed that the steady RANS approach calculates some effects of circumferential grooves on the stall margin even though the flow field itself is unsteady near stall. However, measured increases in stall margin are not well calculated with steady RANS. The flow field in a compressor becomes unsteady near stall due to oscillation of the passage shock and shock/tip clearance vortex interaction. Therefore unsteady flow effects should be considered to investigate the effects of circumferential grooves casing treatment on the

flow structure near stall operation. For the current investigation, an unsteady Reynolds-averaged Navier-Stokes (URANS) approach is applied in addition to steady RANS to investigate flow mechanisms of circumferential grooves casing treatment in a transonic compressor rotor. The results from RANS and URANS are compared with the measured data to understand both steady and unsteady flow effects of the circumferential grooves.

CIRCUMFERENTIAL GROOVES CASING TREATMENT IN AN AXIAL SINGLE-STAGE TRANSONIC COMPRESSOR

Measured data from an axial single-stage transonic compressor with circumferential grooves casing treatment are used for the current investigation. The test rig at the University of Darmstadt, Germany has been used to test many different types of casing treatments along with the latest measurement techniques for compressor flow research.

The design parameters of the high-speed test rig represent a front stage typical of commercial HPCs. The rig has been built for validation of design tools and CFD codes. It also functions as an experimental test bed for new materials and manufacturing methods such as blisks and CRP. The test facility operates in an open circuit; ambient air is sucked into a settling chamber and through a calibrated bell mouth into the stage. Due to the length of the inlet duct and the small volume established at the stage outlet, stall can occur but surge cannot.

The rotor used for all measurements presented herein is the Darmstadt Rotor-1 titanium blisk with 16 radially stacked CDA-profiles. Figure 1 shows the cross section of the single stage axial compressor.

Figure 2 shows six circumferential grooves installed on the compressor casing. Many different casing inserts were manufactured, each representing another configuration of circumferential grooves. The groove onset downstream of the leading edge is at 15.25% of the projected axial chord. Details of the test rotor and the configuration of the grooves are given by Mueller et al. [2007]. For the current study, the flow field with 6 deep grooves shown in Figure 2 is examined in detail. Probes inside the settling chamber were employed to identify the inlet flow conditions. For exit flow measurements, pressure and temperature rakes are mounted on the struts behind the stator. They are equipped with eleven radial sensors each. Therefore, all experimental results are related to the whole stage. Static wall pressure was measured at the same axial position as the rakes at the hub and tip.

RAN, URANS AND CFD GRID

The steady RANS and URANS procedures were applied to obtain steady and unsteady flow fields at various operating conditions. The primary focus of the numerical analysis was to explain the flow mechanism associated with the circumferential grooves casing treatment. Therefore, the isolated rotor configuration with circumferential grooves casing treatment was analyzed numerically. The current compressor stage has a relatively large space between the rotor and the stator, and the upstream influence of stator flow field on the rotor flow field is believed to be relatively minor. The unsteady RANS solutions were used to obtain instantaneous flow structures at near-stall operation. A modified two-equation turbulence model was used for turbulence closure in the RANS methods applied.

In the current study, the governing equations are solved with a pressure-based implicit method using a fully conservative control volume approach. A third-order accurate interpolation scheme is used for the discretization of convection terms and central differencing is used for the diffusion terms. The method is of second-order accuracy with smoothly varying grids. For the time-dependent terms, an implicit second-order scheme is used and a number of sub-iterations are performed at each time step. Details of the RANS method and applications to transonic flows are given by Hah and Wennerstrom [1990].

The computational grid for a single blade passage consists of 98 nodes in the blade-to-blade direction, 75 nodes in the spanwise direction, and 280 nodes in the streamwise direction. The inflow boundary was located 6 average blade heights upstream of the rotor leading edge and the outflow boundary was located one blade height from the trailing edge. The rotor tip clearance geometry is accurately represented by 18 nodes in the blade-to-blade direction, 16 nodes in the spanwise direction, and 140 nodes in the streamwise direction. The circumferential grooves were modeled in a separated block. Each groove is represented by 98 nodes in the circumferential direction and 15 nodes in the radial and axial directions. I-grid topology is used to reduce grid skewness and a single-block grid is used. All the computations were performed with NASA's Columbia super computer system, which allows parallel computation with up to 512 processors.

Standard boundary conditions for an isolated rotor were applied at the boundaries of the computational domain. Circumferentially averaged static pressure at the casing was specified to control the mass flow rate. Non-reflecting boundary conditions were applied at the inlet and the exit boundaries.

MEASURED AND CALCULATED CHANGES IN PRESSURE RISE CHARACTERISTICS DUE TO THE CIRCUMFERENTIAL GROOVES CASING TREATMENT

Figure 3 compares changes in pressure rise characteristics due to a casing treatment with six circumferential grooves from measurements, RANS, and URANS. Measured flow characteristics show that the operating range increases almost 50% with the circumferential grooves casing treatment. It is not easy to measure the exact stalling mass flow rate of a transonic compressor rotor. For this rotor, slightly different stalling mass flow rates have been observed experimentally with different measurement techniques. The currently reported stalling mass flow rate is repeatable and measurement error is estimated to be negligible. It is well known that the magnitude and actual shape of the tip clearance significantly

affect the stall margin of any transonic compressor. Previous numerical analyses of this rotor used a smaller tip gap than the actual value and a wider operating range was observed numerically. The actual measured tip gap is used in the current numerical calculation and the calculated pressure rise characteristics with the actual tip gap are shown in Figure 3. The calculated static pressure distributions at the stall limit with the smooth casing are compared with the measured distributions from the high-response pressure measurement in Figure 4. The overall flow field and detailed shock structures are well calculated with the current numerical approach.

Comparisons in Figure 3 show that steady RANS calculates a stalling mass flow rate for the smooth casing roughly 8% lower than the measured value. On the other hand, steady RANS calculates a flow range extension of only 15% with the circumferential grooves casing treatment while the measurement shows an increase of almost 50%. Previous numerical investigations (for example, Chen et al. [2010]) show a similar trend in calculating stall margin increase due to circumferential grooves casing treatment with steady RANS. The unsteady calculations of circumferential grooves in Figure 3 show an almost 40% increase in stall margin, which is much closer to the measured value. In the following sections, steady and unsteady flow effects are examined with the calculated flow fields at various operating points shown in Figure 3.

STEADY FLOW EFFECTS OF CIRCUMFERENTIAL GROOVES CASING TREATMENT

To examine steady flow effects of the circumferential grooves, calculated flow fields at stall limit with the smooth casing (operating point 1 in Figure 3) are compared with the calculated flow field with the circumferential grooves casing treatment at the same mass flow rate (operating point 2 in Figure 3).

Figure 5 compares static pressure distributions at the rotor tip section. The static pressure distribution with the circumferential grooves shows the influence of grooves especially from the front 3 grooves. The tip clearance vortex is divided into several sections due to the interactions between the main passage flow and flow from/into the grooves. Also, the tip clearance core vortex stays close to the blade suction side with the circumferential casing treatment. Figure 6 compares axial velocity contours. With six circumferential grooves, the low-momentum area near the pressure-side at the leading edge is reduced remarkably compared to the smooth-casing case. In Figure 7, velocity vectors at the rotor tip section are compared. Again, flow blockage near the pressure-side at the leading edge is drastically reduced with the circumferential grooves casing treatment. As observed in previous studies, the circumferential grooves casing treatment defers build up of blockage near the pressure-side leading edge, which results in stable operation at a lower mass flow rate. As discussed in earlier studies on circumferential grooves (for example, Rabe and Hah [2002]), several mechanisms for the delay in blockage build-up are possible. For example,, flow is blown into the grooves near the pressure side of the blade due to the difference in pressure between the main passage near the tip section and the area inside the grooves. On the other hand, flow is injected into main passage from the grooves near the suction side of the blade. These radial flows disrupt the formation of a conventional tip leakage vortex as shown in Figure 5 and prevent low-momentum fluid accumulating near the pressure side of the leading edge.

Figure 8 compares radial velocity distributions at the tip section. Strong radial velocity components are observed with the circumferential grooves casing treatment in Figure 8. Also, segmentation of the tip clearance vortex and relative effects of six individual grooves are clearly shown in Figure 8.

The measured distribution of radial velocity at 92.5% span from PIV (Mueller et al. [2011]) is compared with the calculated distribution in Figure 8. At this radial location, the effects of individual grooves do not show up. The calculated distribution agrees fairly well with the PIV measurements. As shown in Figure 3, steady RANS simulations of circumferential groove casing treatment do not accurately calculate the measured increase of the compressor operating range. The steady simulation indicates only a 10% increase in stall margin while the measurement shows roughly a 50% increase. The flow field becomes unsteady due to the oscillation of the passage shock and the interaction between the shock and the tip clearance vortex. In the following section, possible effects of unsteady flow due to the presence of the circumferential grooves are examined.

UNSTEADY FLOW EFFECTS OF CIRCUMFERENTIAL GROOVES CASING TREATMENT

Numerical investigations of the effects of circumferential grooves have been mostly based on the steady RANS approach (Rabe and Hah [1992], Mueller et al.[2007], Shabbir and Adamczyk [2005], and Chen et al. [2010]). These numerical simulations based on steady RANS show the overall trend of measured aerodynamic benefits of the circumferential grooves casing treatment. However, the steady simulation does not seem to calculate all the measured increase in stall margin as shown in Figure 3. This may be due to the fact that steady RANS does not capture all of the effects of circumferential grooves on the main passage flow. Figure 9 shows changes in instantaneous pressure distribution at near-stall operation on the casing from a high frequency pressure measurement in the Darmstadt's transonic compressor stage (Bergner et al. [2006]). Instantaneous pressure distributions in Figure 9 show significant changes in pressure distribution and tip vortex trajectory. This unsteadiness is mainly due to the interaction between the tip clearance vortex and the passage shock. The measurements indicate that the tip vortex is highly intermittent as the pressure difference across the blade tip section changes.

To include possible effects of the unsteady nature of the flow field at near-stall operation, URANS simulations were performed at several operating points with the 6 deep

grooves configuration of the Darmstadt's transonic rotor. Calculated total pressure rise characteristics from the URANS simulations are shown in Figure 3. The URANS simulation calculates a greater extension of the operating range than the steady RANS simulation, which agrees better with the measurement. The results shown in Figure 3 indicate that there are significant influences of unsteady flow on the performance of the circumferential grooves. This explains why various steady RANS numerical simulations do not calculate the stall margin increase accurately. To examine unsteady flow effects, the calculated flow field at the operating limit from RANS (operating point 3) is compared with the flow field from URANS with the similar mass flow rate (operating point 4).

In Figure 10, static pressure distributions at the rotor tip section are compared. Five thousand instantaneous flow fields are averaged to obtain the averaged solution in Figure 10. Comparison in Figure 10 shows that the tip clearance vortex is further reduced due to the circumferential grooves according to URANS compared to RANS. Pressure contours from URANS show more distinct influences of the grooves compared to RANS results, which indicates a greater influence the of grooves due to unsteady interaction.

Time-averaged axial velocity contours from URANS are compared with those from RANS in Figure 11. Axial velocity contours from URANS show higher axial velocity near the pressure side of the blade, which indicates less accumulation of blockage near the pressure side and stable flow condition at this mass flow rate.

Time-averaged radial velocity contours are compared in Figure 12. Instantaneous distributions of radial velocity contours from URANS at one cycle of vortex oscillation are shown in Figure 13. Although time-averaged radial velocity contours are similar to those from RANS, large changes in radial velocity are observed near the pressure side of the blade.

RMS values of radial velocity components from URANS are shown in Figure 14. Large unsteady changes in radial flow from/into the grooves at this operating point are observed in Figure 14 at the grooves located near the leading edge. It is also interesting to observe large RMS values near the suction side of the blade at the grooves located near the trailing edge. Results shown in Figures 11 and 13 indicate that unsteady flow into/from the grooves energizes flow near the pressure side of the blade, which makes the flow field more stable at this mass flow rate.

Time-averaged relative Mach number distributions at operating point 5 in Figure 3 are compared with the measured distributions from high-response pressure probes in Figure 15 (Mueller et al. [2011]). The calculated location of the passage shock agrees fairly well with the measurement. If the mass flow rate is further reduced by increasing back pressure, the passage shock moves further upstream and flow spillage into the adjacent blade passage can occur due to the blockage at the pressure side of the blade. This prevents stable operation with URANS based on a single-passage simulation. As shown in Figure 3, the calculated increase in stall margin from URANS is about 35% while the measurements show roughly a 50% increase. The difference might be due to the fact that full-annulus effects are not included in the current single-passage simulation and the turbulence model in URANS does not describe the unsteady flow accurately.

CONCLUDING REMARKS

Steady and unsteady flow effects due to circumferential groove casing treatment on the stall margin in a transonic compressor rotor are investigated with steady and unsteady Reynolds-averaged Navier-Stokes simulations. Although steady RANS seem to calculate some qualitative trends correctly, the approach does not seem to calculate the measured increase in stall margin. The present investigation shows that unsteady flow injection from the grooves with axial and radial momentum into the main flow near the casing is a main mechanism in enhancing flow stability and increased stall margin. For the currently investigated transonic compressor, the unsteady effects are roughly twice as large as the steady effects according to the numerical simulations. For certain compressor designs, unsteady effects might be the dominating factor and steady RANS may not calculate any benefits from circumferential grooves. Therefore any optimization strategy of the casing treatment with numerical flow analysis tools should properly include unsteady effects. Although URANS calculates a compressor stall margin much closer to the measured value than the steady RANS, it appears that there is still a significant difference in compressor operating range between them. An even higher fidelity approach (a large eddy simulation or a direct numerical simulation) on the full annulus might be necessary to capture all of the important flow structures for the casing treatment in a compressor.

ACKNOWLEDGMENTS

The author gratefully acknowledge the support of this work by the NASA Fundamental Aeronautics program, Supersonic project.

REFERENCES

Bergner, J., Matthias, K., Schiffer, H. P., and Hah, C., 2006, "Short Length-Scale Rotating Stall Inception in a Transonic Axial Comrpressor - Experimental Investigation," ASME Paper GT2006-90209.

Chen, H., Huang, X., Shi, K., Fu, S., Bennington, M.A., Morris, S.C., Ross, M., McNulty, S., and Wadia, A., 2010, "A CFD Study of Circumferential Groove Casing Treatments in a Transonic Axial Compressor," ASME Paper GT2010-23606.

Crook, A. J., Greitzer, E. M., Tan, C. S., and Adamczyk, J. J., 1993, "Numerical Simulation of Compressor Endwall and Casing Treatment Flow Phenomena," ASME Journal of Turbomachinery, Vol. 115, No. 3, pp. 501-512.

Fujita, H. and Takata, H., 1985, "A Study of Configurations of Casing Treatment for Axial Flow Compressors," Bull. of JSME, Vol. 27, No. 230, pp. 1675-1681.

Hall, E. J., Heidegger, N. J., and Delaney, R. A., 1996, "Performance Prediction of Endwall Treated Fan Rotors with Inlet Distortion," AIAA Paper AIAA 96-0244.

Lee, N. K. W. and Greitzer, E. M., 1990, "Effects of Endwall Suction and Blowing on Compressor Stability Enhancement," ASME Journal of Turbomachinery, Vol. 122, pp. 133-144.

Moore, R. D., Kovich, G., and Blade, R. J., 1971, "Effect of Casing Treatment on Overall and Blade-Element Performance of a Compressor Rotor," NASA TN D-6538.

Mueller, M. W., Schiffer, H. P., and Hah, C., 2007, "Effects of Circumferential Grooves on the Aerodynamic Performance of an Axial Single-Stage Transonic Compressor," ASME Paper GT-2007-27365.

Mueller, M. W., Schiffer, H. P., Voges M. and Hah, C., 2011, "Investigation of Passage Flow Features in a Transonic Compressor Rotor with Casing Treatments," ASME Paper GT-2010-45364.

Paulon, J. and Dehondt, D., 1982, "Influence of Casing Treatment on the Operating Range of Axial Compressors," ASME Paper 82-GT-103.

Prince, D. C. Jr., Wisler, D. C., and Hilvers, D. E., 1974, "Study of Casing Treatment Stall Margin Improvement Phenomena," NASA CR-134552.

Rabe, D. C. and Hah, C., 2002, "Application of Casing Circumferential Grooves for Improved Stall Margin in a Transonic Axial Compressor," ASME Paper GT-2002-30641.

Shabbir. A. and Adamczyk,J.,J., 2005, "Flow Mechanism for Stall Margin Improvement Due to Circumferential Casing Grooves on Axial Compressors," ASME Journal of Turbomachinery, Vol. 127, October 2005, pp. 708-717.

Smith, G. D. J. and Cumpsty. N. A., 1985, "Flow Phenomena in Compressor Casing Treatment," ASME Journal of Engineering for Gas Turbines and Power, Vol. 117, pp. 532-541.

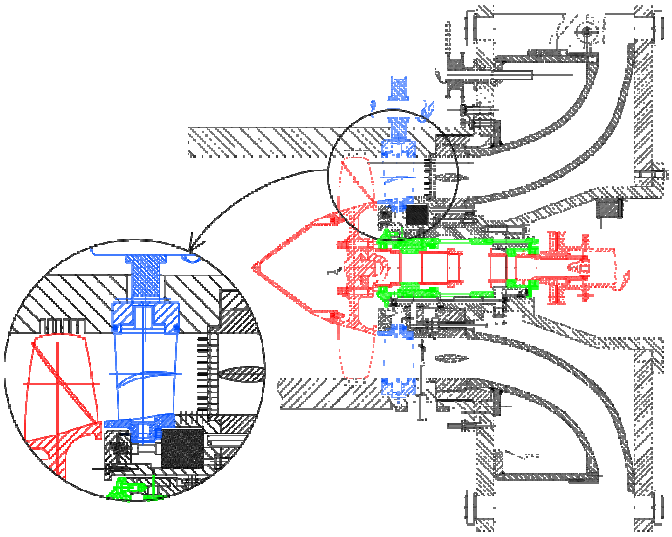

Figure 1: Cross section of Darmstadt transonic compressor stage.

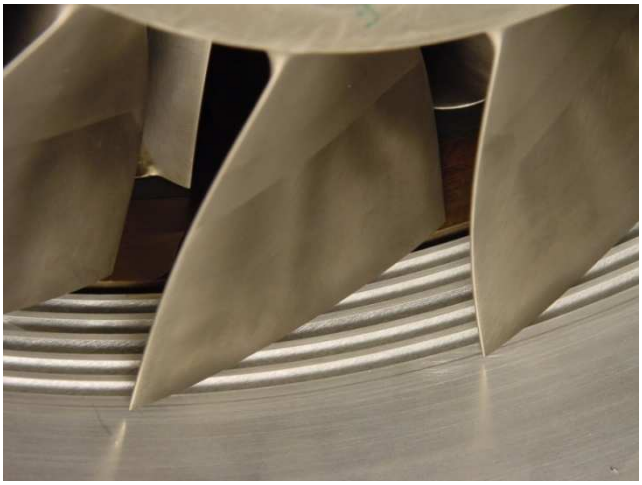

Figure 2: Circumferential casing treatment with six deep grooves.

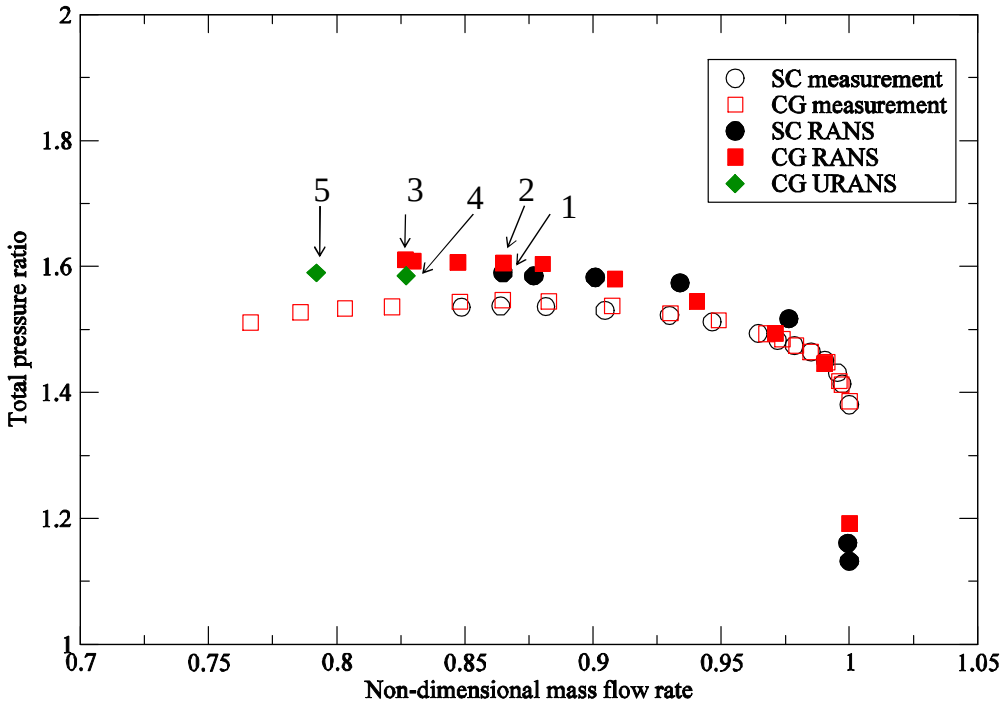

Figure 3: Comparison of total pressure rise at design speed.

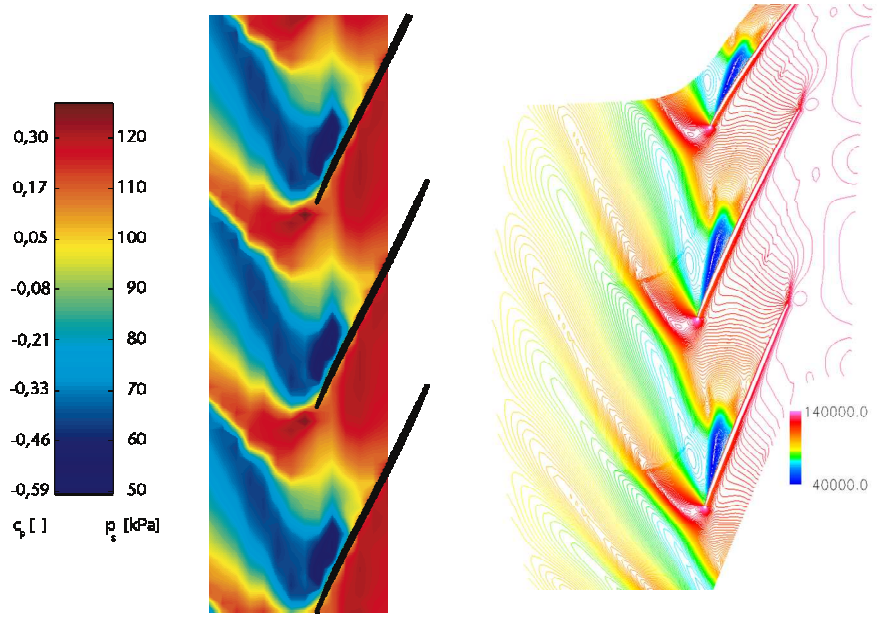

measurement RANS calculation

Figure 4: Comparison of casing static pressure distribution at stall limit with smooth casing.

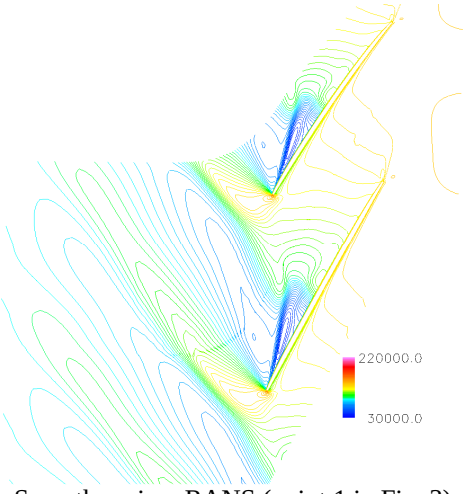

Smooth casing, RANS (point 1 in Fig. 3)

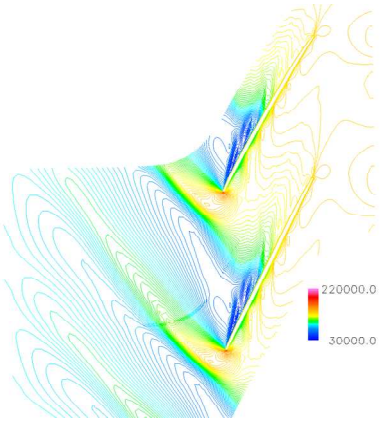

CG RANS at point 2 in Fig. 3

Figure 5: Comparison of static pressure distribution at stall limit, RANS.

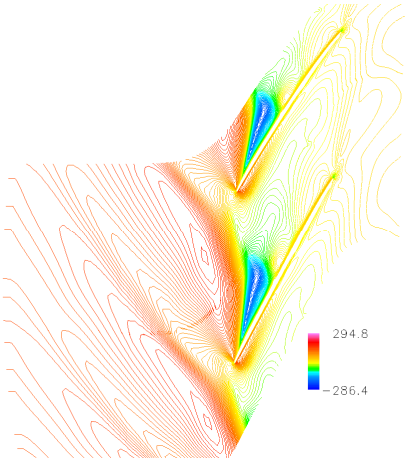

Smooth casing, RANS at point1 in Fig. 3

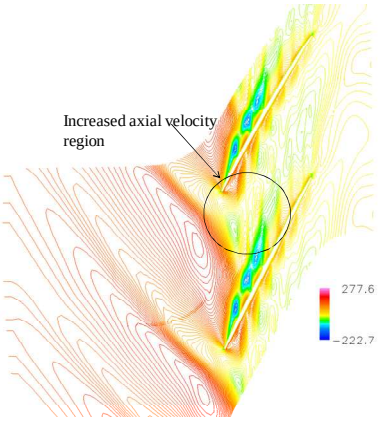

CG RANS at point 2 in Fig. 3

Figure 6: Comparison of axial velocity distribution at stall limit of, RANS.

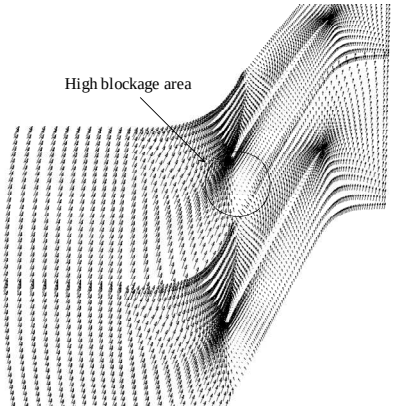

Smooth casing, RANS (point 1 in Fig. 3)

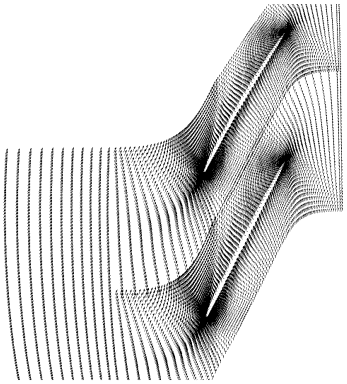

CG RANS at point 2 in Fig. 3

Figure 7: Comparison of velocity vectors at stall limit, RANS.

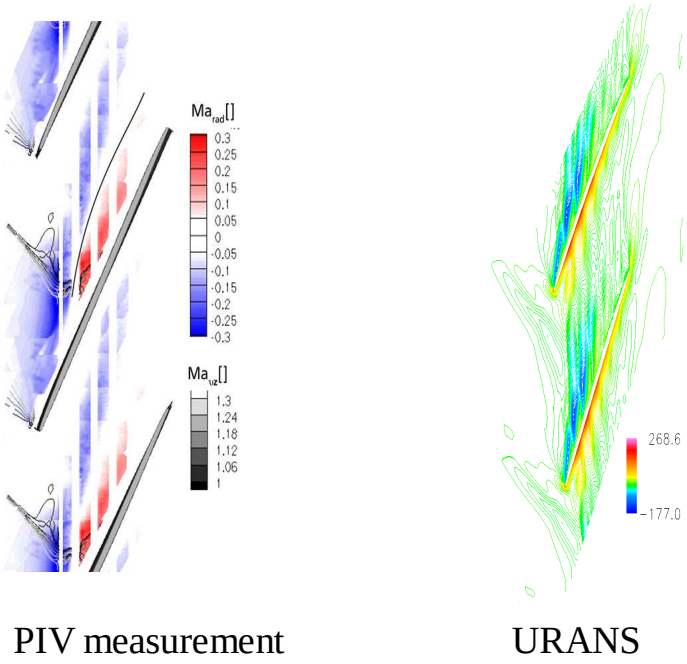

Figure 8: Comparison of radial velocity contours, 92.5 % span at stall limit, RANS.

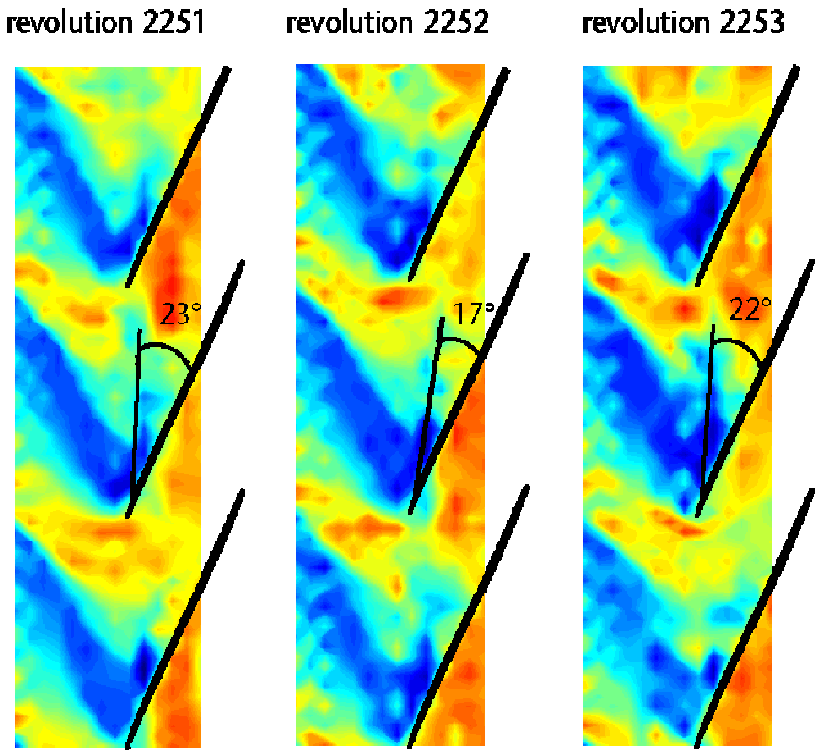

Figure 9: Changes in casing static pressure from high-response static pressure transducer.

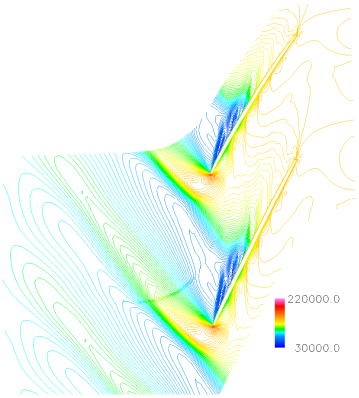

CG RANS, point 3 in Fig.3

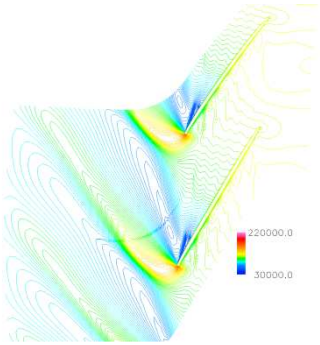

CG URANS, point 4 in Fig.3

Figure 10: Comparison of static pressure distribution at stall limit of CG.

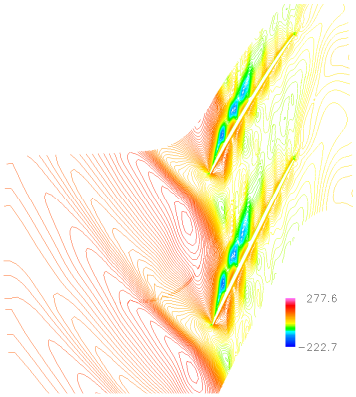

CG RANS, point 3 in Fig.3

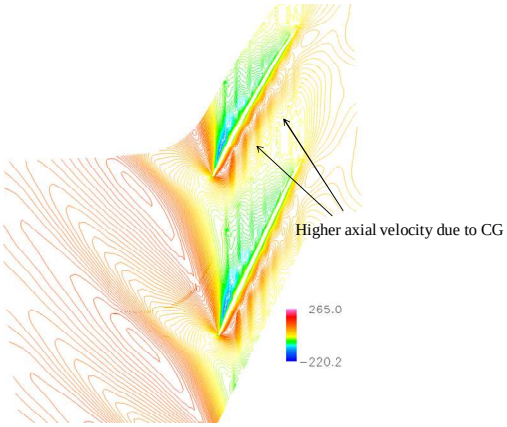

CG URANS, point 4 in Fig. 3

Figure 11: Comparison of axial velocity distribution at stall limit of CG.

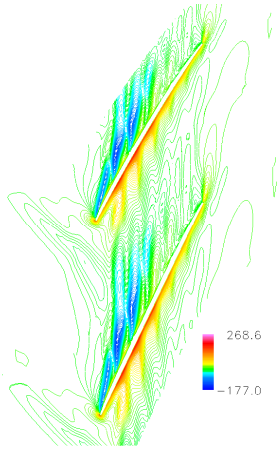

CG RANS, point 3 in Fig.3

CG URANS, point 4 in Fig. 3

Figure 12: Comparison of radial velocity distribution at stall limit of CG.

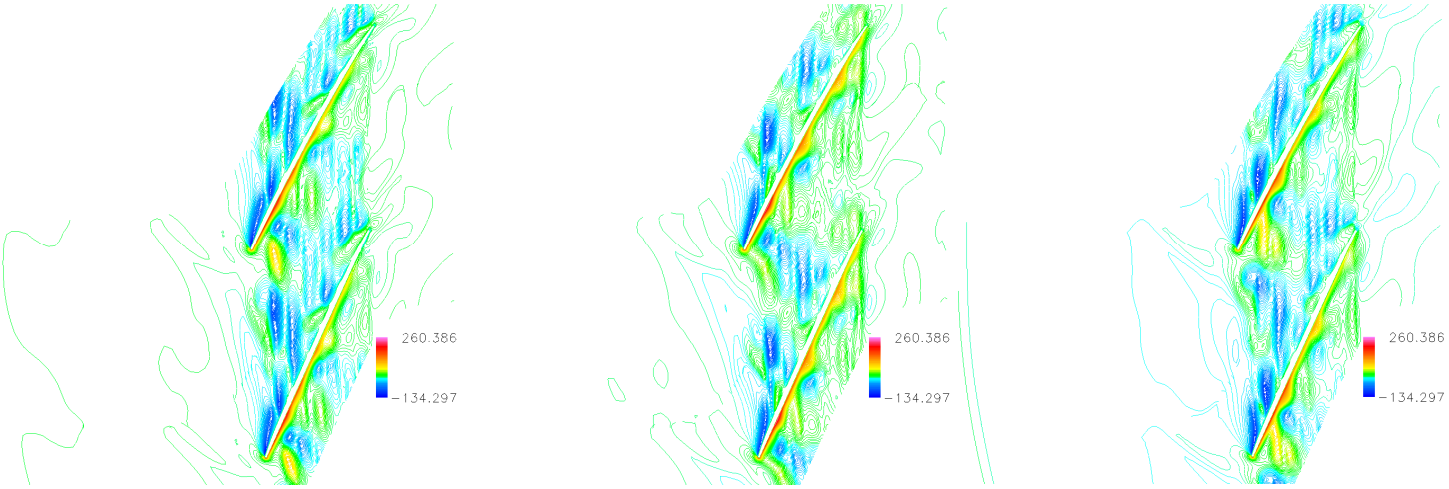

Time step 1 Time step 2 Time step 3

Figure 13: Changes of radial velocity distribution from URANS, at point 4 in Fig. 3.

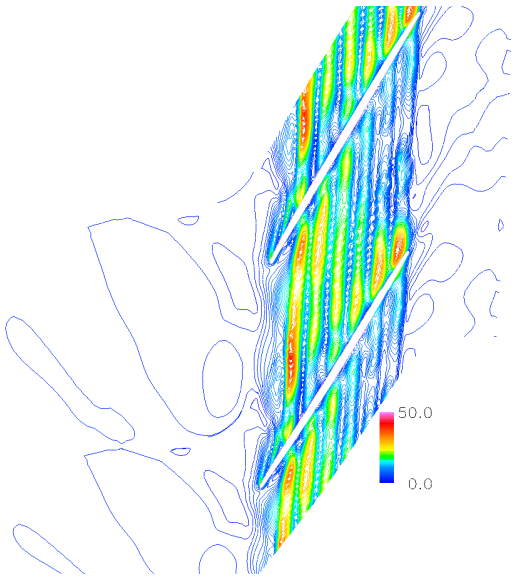

Figure 14: Distribution of RMS values of radial velocity from URANS.

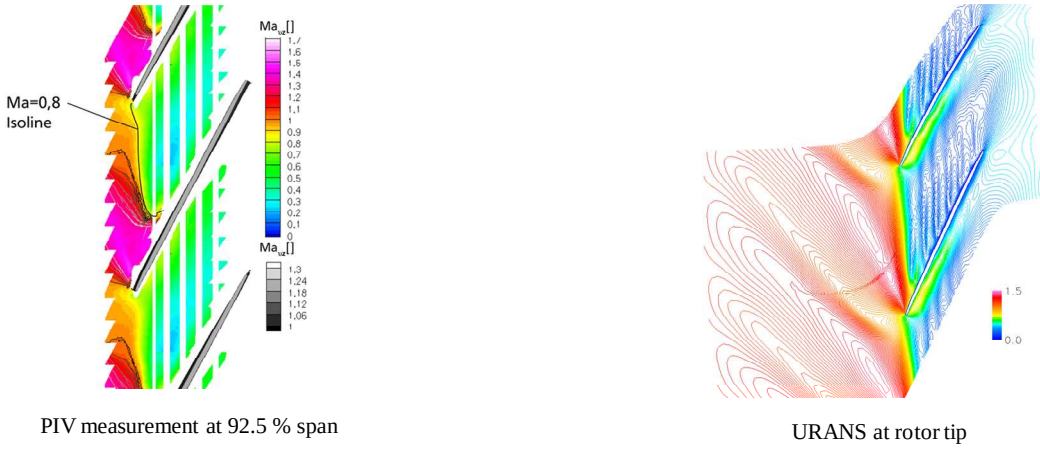

PIV measurement at 92.5 % span URANS at rotor tip

Figure 15: Comparison of Mach number distributions at stall limit with circumferential grooves casing treatment, operating point 5 in Fig. 3.